Water Research 305 (2026) 126544

Contents lists available at ScienceDirect

Water Research

journal homepage: www.elsevier.com/locate/watres

Hydrological inundation threshold regulates the carbon source-sink transition in unvegetated tidal flats

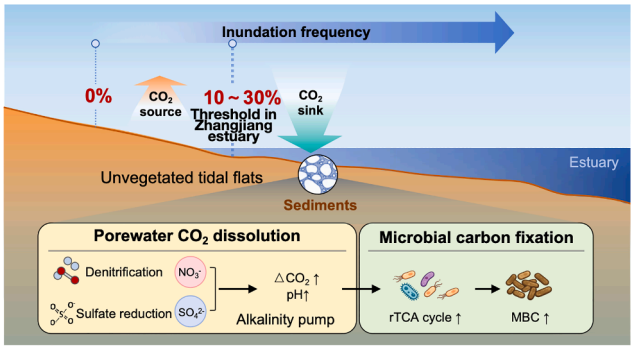
Hui Wu [a,b,c], Yasong Chen [b,c], Shiyao Chen [a,b,c], Mengru Li [a,b,c], Yihui Zhang [b,c], Mingliang Zhao [d], Guangxuan Han [d], Nengwang Chen [a,b,c,*]

[a] Fujian Provincial Key Laboratory for Coastal Ecology and Environmental Studies, College of the Environment and Ecology, Xiamen University, Xiamen, 361102, China
[b] State Key Laboratory of Marine Environmental Science, College of the Environment and Ecology, Xiamen University, Xiamen, 361102, China
[c] National Observation and Research Station for the Taiwan Strait Marine Ecosystem, Xiamen University, Zhangzhou, 363000, China
[d] Key Laboratory of Coastal Zone Environmental Processes and Ecological Remediation, Yantai Institute of Coastal Zone Research, Chinese Academy of Sciences, Yantai, 264003, China

HIGHLIGHTS

- An inundation threshold controls CO_2 source-sink shifts in unvegetated tidal flats.
- Denitrification and sulfate reduction enhance CO_2 dissolution by alkalinity pump.
- Inundation enhances microbial carbon fixation through rTCA cycle in sediments.

GRAPHICAL ABSTRACT



ARTICLE INFO

Keywords:
Blue carbon
Unvegetated tidal flats
Greenhouse gases
Climate mitigation
Estuary

ABSTRACT

Unvegetated tidal flats cover extensive areas of global coastlines, but their role in atmospheric CO_2 exchange remains poorly understood. Here we investigate how hydrological regimes regulate carbon uptake in these ecosystems through a marsh organ experiment in the subtropical Zhangjiang Estuary, China that integrated sediment-atmosphere CO_2 and CH_4 flux measurements, porewater geochemistry, and metagenomic sequencing. We identified a site-specific hydrological transition in which sediment-atmosphere CO_2 exchange shifted from a weak source to sustained net uptake under more frequent inundation, with the transition occurring around an annual inundation frequency of approximately 10-30% in this experimental system. This transition coincided with declining porewater NO_3^-/Cl^- and SO_4^{2-}/Cl^- ratios and increasing pH, dissolved CO_2 concentration, and carbonate system derived estimated alkalinity, consistent with enhanced anaerobic redox processes and alkalinity-associated CO_2 dissolution and retention. Although CH_4 emissions increased under frequent inundation, incorporating CH_4 into global warming potential did not substantially offset the CO_2 sink transition. Metagenomic analyses further showed an enrichment of rTCA-related carbon-fixation taxa under frequent

* Corresponding author at: Fujian Provincial Key Laboratory for Coastal Ecology and Environmental Studies, College of the Environment and Ecology, Xiamen University, Xiamen, 361102, China.
E-mail address: nwchen@xmu.edu.cn (N. Chen).

https://doi.org/10.1016/j.watres.2026.126544
Received 24 March 2026; Received in revised form 20 June 2026; Accepted 20 July 2026
Available online 21 July 2026
0043-1354/© 2026 Elsevier Ltd. All rights are reserved, including those for text and data mining, AI training, and similar technologies.

inundation, indicating greater microbial autotrophic carbon-fixation potential. This functional potential was associated with porewater geochemical changes and increased microbial biomass carbon, supporting the possibility of hydrologically modulated geochemical-microbial coupling during the CO_2 source-sink transition. Together, our results unveil a previously unrecognized mechanism in which a hydrologically-modulated geochemical-microbial coupling drives CO_2 uptake in frequently inundated sediments. These findings extend current blue carbon frameworks by highlighting the previously overlooked role of unvegetated tidal flats in coastal carbon cycling and climate regulation.

1. Introduction

Unvegetated tidal flats cover an estimated 127,921 km^2 globally (Murray et al., 2019), an area comparable to mangroves and approximately 2-3 times larger than salt marshes, representing nearly one quarter of global coastal blue carbon ecosystems (Davidson and Finlayson, 2019). Despite their extensive spatial coverage and substantial sediment carbon pools (Lin et al., 2020), their role in regulating atmospheric carbon exchange remains poorly constrained. Unlike vegetated coastal wetlands, tidal flats lack vascular plant productivity and are therefore commonly assumed to function primarily as net CO_2 sources driven by sediment organic matter mineralization (Chen and Lee, 2024). This assumption has limited the understanding of carbon exchange in unvegetated tidal flats and contributed to their omission from blue carbon assessments (Bertram et al., 2021; Macreadie et al., 2019).

Recent observations challenge this assumption. Several field and mesocosm studies have reported reduced CO_2 emissions or even negative CO_2 fluxes under increased inundation conditions in tidal flats and coastal sediments (Douglas et al., 2025; Hamilton et al., 2020; Krauss et al., 2016). Tidal hydrology is one of the most fundamental physical drivers regulating biogeochemical processes in intertidal environments (Shahan et al., 2022). Even small variations in surface elevation can substantially alter tidal inundation frequency and duration, thereby influencing sediment moisture, redox conditions, and microbial metabolic pathways (Alongi, 2014; Lovelock et al., 2015). In vegetated coastal wetlands, increasing inundation has been widely shown to suppress sediment respiration and reduce ecosystem CO_2 emissions (Megonigal et al., 2003). These findings suggest that hydrological forcing may fundamentally alter carbon exchange processes in unvegetated coastal sediments. However, the mechanisms underlying such shifts remain unresolved. In particular, the existence of a hydrological threshold that regulates the transition of tidal flats from CO_2 sources to sinks has not been directly demonstrated.

Several mechanisms may contribute to potential CO_2 uptake in unvegetated tidal flats. First, benthic microalgae and microphytobenthos (MPB) can fix inorganic carbon through photosynthesis during tidal exposure (MacIntyre et al., 1996). Second, anaerobic mineralization processes can alter the carbonate system through the production of alkalinity (Hu and Cai, 2011; Sulpis and Middelburg, 2023). During tidal inundation, sediments rapidly shift toward reducing conditions, where microorganisms sequentially utilize alternative electron acceptors such as nitrate, iron, manganese, and sulfate to decompose organic matter (Candry et al., 2023). These reactions generate bicarbonate and increase total alkalinity, lowering porewater pCO_2 and thereby promoting atmospheric CO_2 dissolution through a geochemical alkalinity pump (Middelburg et al., 2020). Third, chemolithoautotrophic microorganisms may assimilate CO_2 into biomass through dark carbon fixation pathways (Middelburg, 2011). Despite these proposed pathways, it remains unclear whether tidal hydrological forcing can systematically regulate these processes in unvegetated tidal flats and ultimately drive net atmospheric CO_2 uptake at the sediment–atmosphere interface. In particular, the potential coupling between alkalinity production and microbial carbon fixation under varying inundation regimes has rarely been examined.

Microbial carbon fixation has increasingly been recognized as an important yet often overlooked component of sediment carbon cycling (Qi et al., 2023). Aerobic and facultative autotrophic microorganisms typically fix CO_2 through the Calvin-Benson-Bassham (CBB) cycle catalyzed by Rubisco (Berg, 2011). In contrast, alternative autotrophic pathways such as the reductive tricarboxylic acid (rTCA) cycle and the Wood-Ljungdahl (W-L) pathway require substantially less energy and are thermodynamically favored under reducing conditions, making them common among anaerobic and facultatively anaerobic microorganisms (Fuchs, 2011; Steffens et al., 2021). At the same time, microbial respiration releases CO_2, meaning that the composition and metabolic strategies of microbial communities ultimately determine the net direction of CO_2 exchange (Falkowski et al., 2008). However, whether hydrological forcing can systematically shift microbial carbon fixation pathways toward more energy-efficient metabolisms, thereby enhancing carbon allocation to biomass, remains largely unexplored.

Based on these considerations, we hypothesize that tidal inundation may cause a coupled geochemical-microbial mechanism that enhances CO_2 uptake in unvegetated tidal flats. To test this hypothesis, we conducted an elevation-controlled marsh organ experiment combined with gas flux measurements, porewater geochemistry, and metagenomic analyses. Our objectives were to: (1) determine whether a sediment-atmosphere CO_2 source-sink transition occurs along the inundation gradient and identify its potential threshold range; and (2) elucidate the coupled biogeochemical mechanisms linking hydrological forcing, porewater CO_2 dissolution, and microbial carbon metabolism. By revealing how tidal inundation reorganizes sediment carbon cycling processes, this study provides mechanistic insights into CO_2 uptake in unvegetated intertidal sediments and extends vegetation-centered blue carbon frameworks.

2. Materials and methods

2.1. Design and sampling of an in-situ marsh organ

An *in-situ* marsh organ experiment was established in the Zhangjiang Estuary, Fujian Province, China (23°56′37″ N, 117°22′43″ E), to manipulate sediment inundation frequency along an elevation gradient (Fig. S1a) (J. Wang et al., 2025). The region experiences a subtropical monsoon climate with a mean annual temperature of 21.1°C (Zhu et al., 2025) and irregular semidiurnal tides. Seawater salinity averages approximately 10 PSU but fluctuates daily between 0 and 18 PSU.

Five elevation treatments (150, 100, 50, 0, and -50 cm relative to mean sea level) were established, corresponding to annual inundation frequencies of approximately 2%, 12%, 28%, 47%, and 65%, respectively, with mean sea level (MSL) serving as a unified vertical datum for deriving comparable inundation frequencies across treatments (Fig. 1 A; Text S1). Three PVC cylinders filled with sediment collected from the surrounding tidal flat were installed at each elevation level. The sediments were classified as clay loam (Fig. S1b).

The marsh organ experiment was deployed on 7 April 2023 and allowed to incubate in situ for one year (Fig. 1 B, C; Text S1). Sediment-atmosphere CO_2 and CH_4 fluxes were measured, and surface sediment and porewater samples were collected during low tide on 13 April (Dry season) and 9 July 2024 (Wet season). Surface sediments (0-2 cm) were collected using a hand shovel and immediately sealed in sterile polyethylene bags. The samples were placed in insulated containers with ice

packs during transport. Porewater samples were collected using Rhizon samplers (Rhizosphere Research Products, Netherlands) inserted diagonally into the sediment. Approximately 5 mL of porewater was extracted using a syringe connected to a three-way valve under vacuum pressure and stored in pre-combusted glass vials (550°C for 5 h). All samples were collected within two hours after tidal exposure. Sediment samples were stored at -80°C for microbial and physicochemical analyses, while porewater samples were stored at 4°C and processed within 24 h.

2.2. Sediment-atmosphere CO_2 and CH_4 flux measurements

Sediment-atmosphere CO_2 and CH_4 fluxes were measured using a trace gas analyzer (LI-7810, LI-COR Biosciences, USA) connected to a Smart Chamber (8200-01S, LI-COR Biosciences, USA). The chamber was placed onto pre-installed acrylic collars (height 11 cm, diameter 21 cm) inserted into the sediment prior to measurements. Each measurement lasted 180 s and was repeated three times with a 20 s interval between measurements. During each deployment, second-by-second concentrations of CO_2 and CH_4 were continuously recorded. Gas fluxes were calculated using SoilFluxPro software (LI-COR Biosciences) based on the linear rate of change in gas concentration over time. The first and last ~40 s of data were excluded to minimize chamber disturbance effects, and the remaining data were fitted using linear regression to estimate flux rates (Su et al., 2024).

2.3. Sediment and porewater geochemical analyses

Dissolved CO_2 in porewater was determined using a headspace equilibration method modified from Cotovicz et al. (2024). Briefly, 5 mL of porewater was equilibrated with 22 mL of high-purity N_2 in a 27 mL pre-evacuated amber glass vial by shaking at 180 rpm for 30 min. After equilibration, headspace CO_2 concentration was measured using a gas chromatograph (Agilent 7890A, USA). The dissolved CO_2 concentration was calculated using a Henry's law-based mass-balance equation that accounted for headspace and water volumes, equilibration temperature, salinity-dependent CO_2 solubility, and headspace CO_2 concentration.

Porewater pCO_2 was calculated from the dissolved CO_2 concentration using the temperature- and salinity-corrected CO_2 solubility coefficient (Weiss, 1974). Carbonate system calculations were then performed using the CO2SYS program with measured pH and pCO_2 as input parameters, together with sample-specific salinity and temperature (Lewis and Wallace, 1998). The carbonate-system-derived alkalinity is hereafter referred to as estimated alkalinity, and was used to evaluate relative changes in porewater carbonate chemistry among elevation treatments rather than as a direct measurement of total alkalinity.

SWC was determined from the mass difference between freeze-dried and fresh sediments relative to wet weight. Microbial biomass carbon (MBC) was measured using the chloroform fumigation extraction method (Liu et al., 2017; Test S2). Porewater nitrate (NO_3^-) concentrations were determined using an automated nutrient analyzer (AA3, SEAL Analytical, Germany) (Wang et al., 2023). Sulfate (SO_4^{2-}), chloride (Cl^-), calcium (Ca^{2+}), and magnesium (Mg^{2+}) were measured by ion chromatography (ICS-1100, Thermo Fisher Scientific, USA). Porewater pH was measured with a multiparameter water quality meter (Multi 3630 WTW, Germany). DOC concentration was determined using a TOC-V CPN total organic carbon analyzer (Shimadzu, Japan) according to Lu et al. (2023).

To assess the bioavailability of dissolved organic carbon (BDOC), porewater was extracted from sediments by centrifugation following previously described methods (Dong et al., 2026). One subsample was immediately analyzed for DOC concentration and optical properties, while another was incubated in 12 mL amber glass vials without headspace at *in-situ* temperature (32°C) in the dark for 30 days to determine refractory dissolved organic carbon (RDOC). This incubation period was based on previous studies showing that BDOC is largely consumed within 5-30 days (Lian et al., 2021). BDOC was calculated as the difference between DOC and RDOC concentrations.

Dissolved organic matter (DOM) fluorescence was measured using a spectrofluorometer (Aqualog, HORIBA Scientific, Japan). Parallel factor analysis (PARAFAC) identified two dominant fluorescent components (Fig. S2): a protein-like component (C1) (Jørgensen et al., 2011) and a humic-like component (C2) (Guo et al., 2011). Detailed sample processing, analytical procedures, and quality control are described in Supplementary Text S2.

2.4. DNA extraction and shotgun metagenomic sequencing

Total genomic DNA of the sediment samples was extracted utilizing the HiPure Soil DNA Kit B (Magen, China). DNA quality and concentration were assessed using a NanoDrop and a Qubit 4 Fluorometer (Thermo Scientific, USA), respectively. Shotgun metagenomic sequencing was performed on the MGIseq-T7 platform, generating an

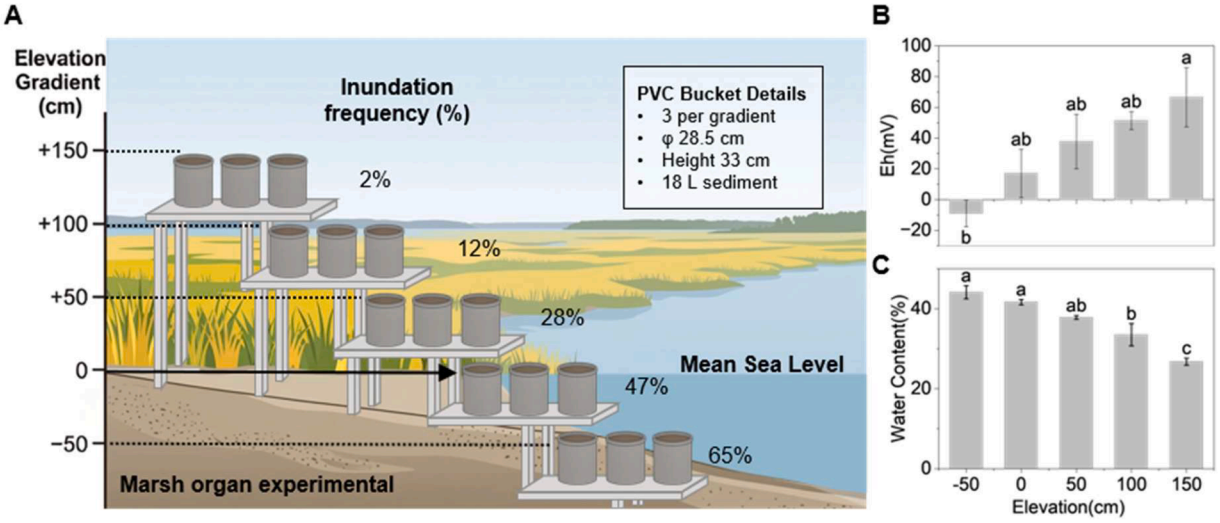


Fig. 1. Schematic diagram of the marsh organ and environmental factors. (A) Relationship between elevation treatments and annual inundation frequency. (B) Relationship between elevation treatments and oxidation reduction potential (Eh) and (C) water content. Bars represent mean ± standard error (SE). Different letters indicate significant differences among treatments (one-way ANOVA followed by Tukey' s HSD test, $P < 0.05$).

average of 50 Gbp paired-end reads per sample (Table S1). Metagenomic data processing generally followed Fan et al. (2024). Briefly, quality-filtered reads were assembled, binned, refined, and dereplicated to recover MAGs. MAGs with completeness >50% and contamination <10% were retained, yielding 554 unique clusters after dereplication at 95% average nucleotide identity. MAG abundance, taxonomy, and carbon-fixation pathways were determined using CoverM, GTDB-Tk, and METABOLIC, respectively, identifying 20 MAGs associated with carbon-fixation potential (Table S2; Text S3).

2.5. Data analysis

All statistical analyses were performed using R (v4.5.1) with RStudio (2025.09.1+401). Figures were generated using Origin 2025 (OriginLab Corporation, USA). Differences among elevation treatments were tested using one-way analysis of variance (ANOVA) followed by Tukey's post hoc test when significant effects were detected. Bar plots present mean values with standard errors (SE). CH_4 fluxes were converted to CO_2 equivalents using a 100-year global warming potential (GWP) factor of 27.9 and then incorporated into the total GWP calculation.Linear regression analyses were conducted after removing studentized outliers. Redundancy analysis (RDA) was performed using the vegan and rdacca.hp packages. Random forest (RF) analysis was conducted using the randomForest and rfPermute packages. Partial least-squares structural equation modeling (PLS-SEM) was performed using the plspm package. Further details are provided in Text S4.

3. Results

3.1. Sediment-atmosphere CO_2 and CH_4 fluxes and potential production rates

Sediment-atmosphere CO_2 fluxes were measured in April 2024 (dry season) and July 2024 (wet season). During the two sampling campaigns, seawater temperatures were 23.7°C and 32.0°C, respectively. Seawater salinity was 8.30 in the dry season and 0.25 in the wet season, while porewater salinity was 12.0 and 2.0, respectively.

CO_2 fluxes decreased progressively with decreasing elevation and shifted from a net source to a net sink between 50 and 100 cm elevation in both seasons, corresponding to an annual inundation frequency range of approximately 12-28% (Fig. 2 A). In the dry season, fluxes declined from 320 ± 223 mg C m^{-2} d^{-1} at the highest elevation to -4739 ± 982 mg C m^{-2} d^{-1} at the lowest elevation. In the wet season, CO_2 fluxes decreased from 350 ± 187 mg C m^{-2} d^{-1} to -2398 ± 1215 mg C m^{-2} d^{-1} along the elevation gradient. Potential CO_2 production rates were measured using sediment slurry incubations. Potential CO_2 production rates in the dry season (-0.16 ± 0.23 to 1.09 ± 0.25 μg C g^{-1} dry weight d^{-1}) were significantly lower than those in the wet season (1.86 ± 0.13 to 4.80 ± 0.68 μg C g^{-1} dry weight d^{-1}). Production rates exhibited a nonlinear relationship with elevation, with the highest values occurring at 100 cm elevation (Fig. 2 B).

CH_4 fluxes exhibited pronounced seasonal differences (Fig. 2 C). During the dry season, CH_4 fluxes were generally low (-104 ± 46 to 173 ± 271 μg C m^{-2} d^{-1}) and showed no significant variation along the elevation gradient ($P > 0.05$). In the wet season, CH_4 fluxes were substantially higher and increased with decreasing elevation. Nevertheless, the magnitude of CH_4 fluxes remained much lower than that of CO_2 fluxes after unit conversion. When CH_4 emissions were incorporated into CO_2-equivalent global warming potential, the hydrological source-sink transition remained broadly similar to that based on CO_2 fluxes alone (Fig. S4 B). Potential CH_4 production rates were substantially lower than CO_2 production rates and showed no significant variation across seasons or along the elevation gradient (Fig. 2 D).

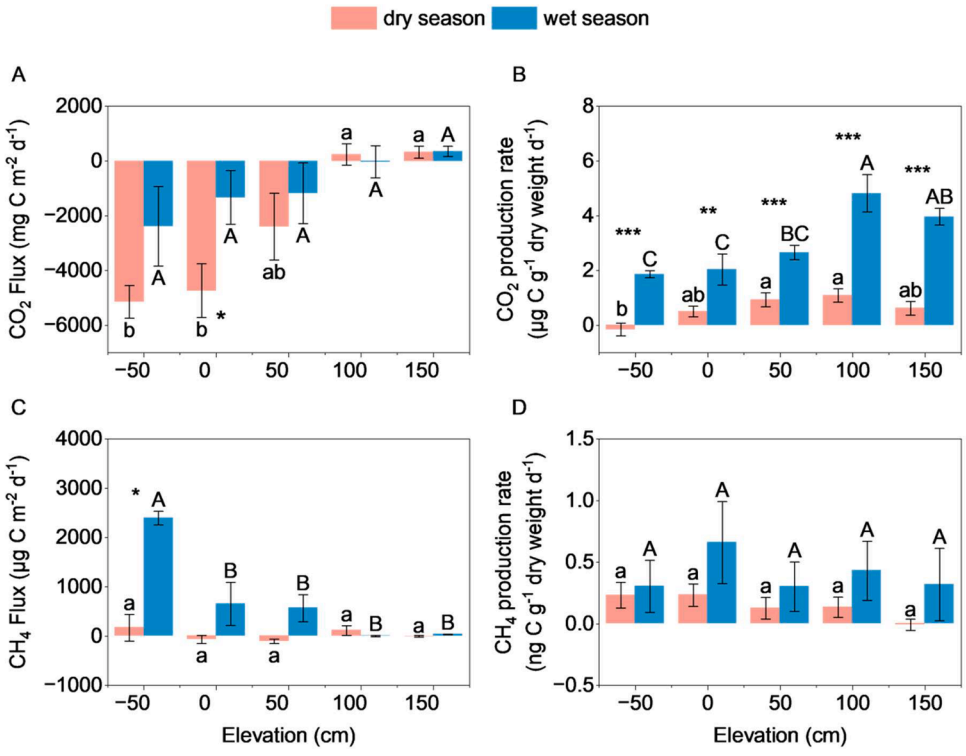


Fig. 2. Changes in sediment-atmosphere interface CO_2 and CH_4 fluxes and potential production rates along the elevation gradient in the marsh organ. (A) CO_2 flux; (B) Potential CO_2 production rate; (C) CH_4 flux; (D) Potential CH_4 production rate. Bars represent mean ± standard error (SE). Uppercase and lowercase letters indicate significant differences along the elevation during the rainy season and dry season, respectively. Asterisks indicate significant differences between the two observation periods at the same elevation treatment.

3.2. Physicochemical properties of sediments and porewater

The molar ratio of SO_4^{2-}/Cl^- in porewater was positively correlated with elevation (Fig. 3 B). In the dry season, the ratio increased from 0.94 at -50 cm elevation to >1.5 at 100-150 cm elevations. In the wet season, SO_4^{2-} was strongly depleted relative to Cl^-, resulting in SO_4^{2-}/Cl^- ratios that were one to two orders of magnitude lower than in the dry season (0.027 to 0.54). In contrast, NO_3^-/Cl^- ratios remained extremely low (<0.01) during both sampling campaigns due to the very low NO_3^- concentrations in porewater (0.14-0.64 μmol L^{-1}), which were substantially lower than NO_3^- concentrations in the surrounding seawater at the time of sampling (114.5-202.6 μmol L^{-1}) (Fig. 3 A). In the dry season, the NO_3^-/Cl^- ratio showed a slight increase with elevation.

Porewater carbonate chemistry showed elevation-dependent patterns (Fig. 3 C-F). In both seasons, porewater pH, dissolved CO_2 concentration, and estimated alkalinity generally increased with decreasing elevation. Seasonal differences were also evident. Overall, porewater pH and estimated alkalinity were higher in the dry season (pH: 6.3-7.7) than in the wet season (pH: 6.0-6.7). Estimated alkalinity was derived from carbonate-system calculations and is therefore interpreted primarily in terms of relative treatment-level patterns rather than absolute values. Dissolved CO_2 concentrations showed overlapping seasonal ranges, varying from 100-812 μmol L^{-1} in the dry season and 179-1030 μmol L^{-1} in the wet season. The combined Ca^{2+} and Mg^{2+} concentration were lower in the dry season (20.6 ± 1.9 μmol L^{-1}) than in the wet season (36.2 ± 2.1 μmol L^{-1}), with no significant variation along the elevation gradient.

MBC generally increased with decreasing elevation, ranging from 166.2 ± 45.5 mg kg^{-1} to 322.9 ± 51.4 mg kg^{-1} (Fig. 4 A). DOC concentrations ranged from 1123.5 to 1830.0 μmol L^{-1} (Fig. 4 B). The BDOC/DOC ratio increased significantly with decreasing elevation ($P < 0.01$), ranging from 10.1% to 74.5% (Fig. 4 C), suggesting that a large fraction of porewater DOC was potentially available for microbial utilization. The ratio of fluorescence component changes derived from incubation experiments (ΔC1/|ΔC2|, defined as the increase in humic-like components relative to the decrease in protein-like components) exhibited a nonlinear relationship with elevation (Fig. 4 D).

3.3. Microbial community structure and functional pathways

The community composition of microorganisms carrying different carbon fixation pathways (Text S5, Fig. 5 A), represented by TPM values of individual MAGs, showed clear shifts along the elevation gradient and was associated with porewater geochemical conditions. In particular, the MAG carrying rTCA cycle related functional genes (Nitrospirota, bin.11) showed high abundance in low-elevation sediments (-50 to 50 cm elevation) and was positively associated with pH and MBC, but negatively associated with SO_4^{2-}/Cl^-, NO_3^-/Cl^- ratios(Fig. 5C). Similarly, microorganisms carrying the W-L pathway (Nitrospirota; bins 8-10 and 12) peaked below 50 cm, and their abundances were associated with porewater SO_4^{2-}/Cl^- and NO_3^-/Cl^- ratios. In contrast, most genomes carrying the CBB cycle, particularly Pseudomonadota (bins 13 and 17-20), maintained high abundances across all elevations (TPM > 1000). However, populations affiliated with Chloroflexota (bin 6) and a subset of Pseudomonadota (bins 15 and 16) were negatively correlated with SWC and were enriched at the highest elevation.

In addition to carbon fixation pathways, taxonomic annotation of these MAGs also revealed key microbial groups with potential roles in nitrogen and sulfur cycling (Fig. 5 A; Table S2). An ammonia-oxidizing bacterium affiliated with Nitrosomonas (bin 13) showed the highest abundance in treatments with stronger inundation (-50 to 50 cm elevation). Several highly abundant MAGs (bins 8-12) were classified as Nitrospira related or comammox Nitrospira MAGs. Furthermore, genomes affiliated with the sulfur-oxidizing Thiohalophilaceae (bin 15) and the sulfate-reducing Thermodesulfovibrionales (bin 7) were identified, suggesting potential coupling between sulfur reduction processes and microbial CO_2 fixation.

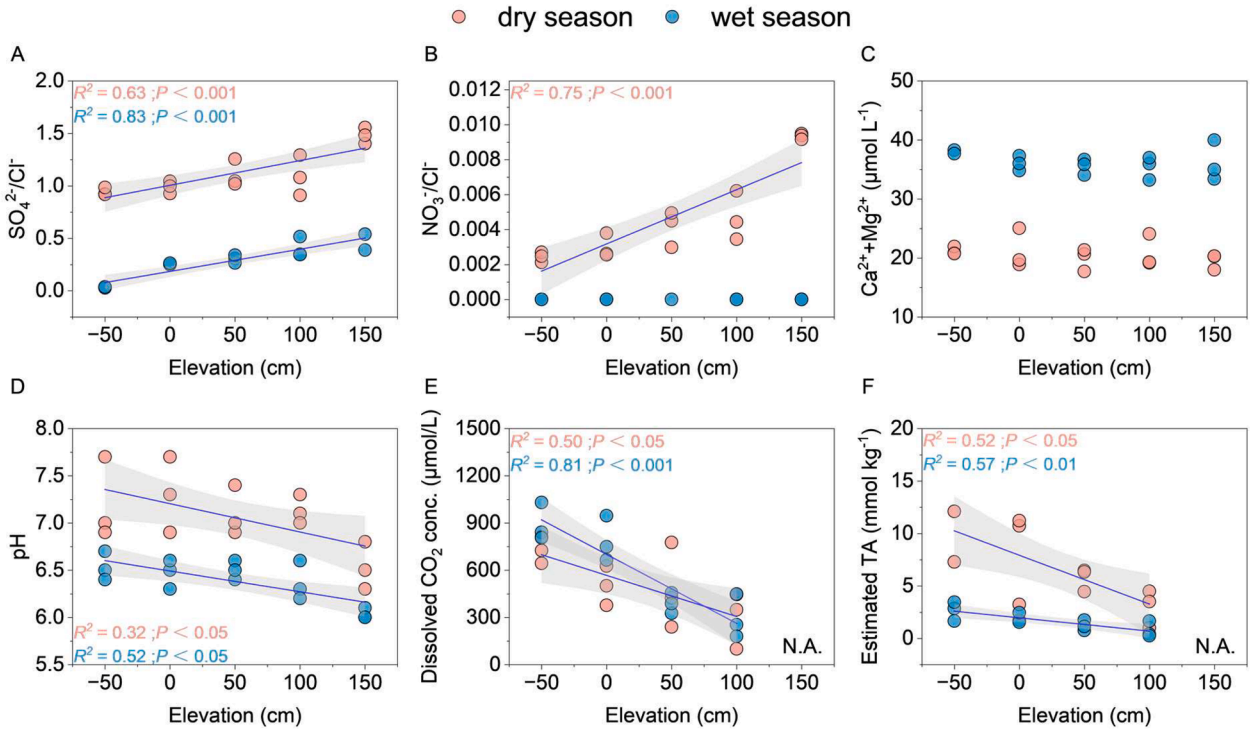


Fig. 3. Seasonal variations in sediment porewater geochemical parameters along the elevation gradient. (A) NO_3^-/Cl^-; (B) SO_4^{2-}/Cl^-; (C) Ca^{2+} + Mg^{2+} concentration; (D) pH; (E) Porewater dissolved CO_2 concentration; (F) Estimated total alkalinity (TA). The blue line is the fitted line, and the gray shaded area represents the 95% confidence interval.

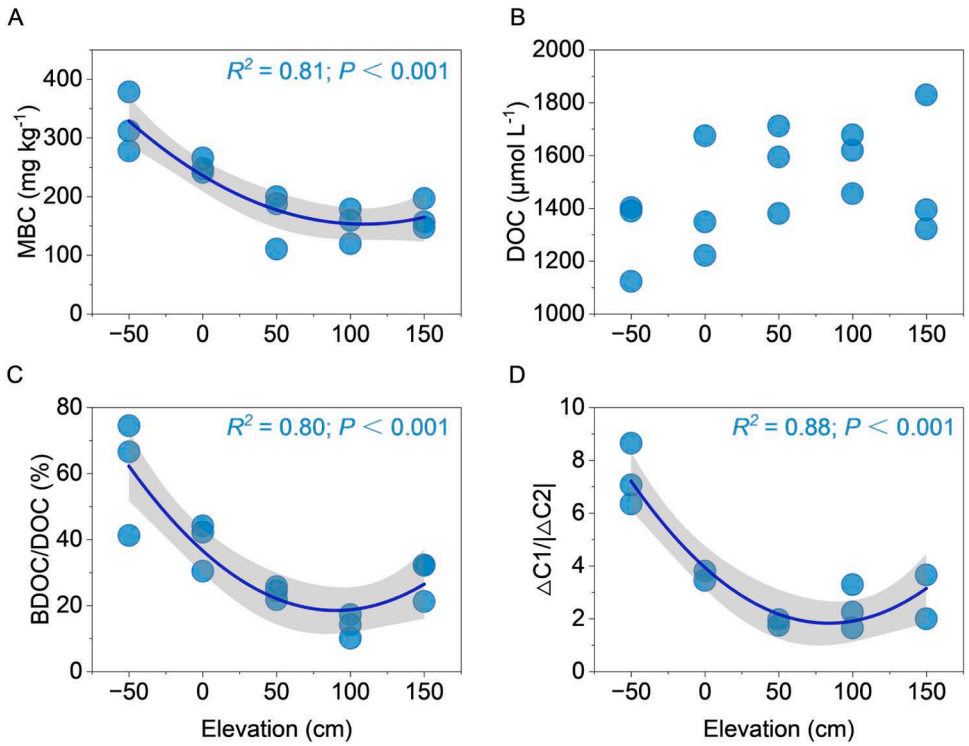


Fig. 4. Key characteristic indicators of the sediment organic carbon pool. (A) Microbial biomass carbon (MBC); (B) Dissolved organic carbon (DOC); (C) Ratio of bioavailable dissolved organic carbon to total dissolved organic carbon (BDOC/DOC); (D) Ratio of the increase in humic-like components to the decrease in protein-like components (ΔC1/|ΔC2|). The results were obtained from sampling conducted in July 2024 at the end of the experiment.

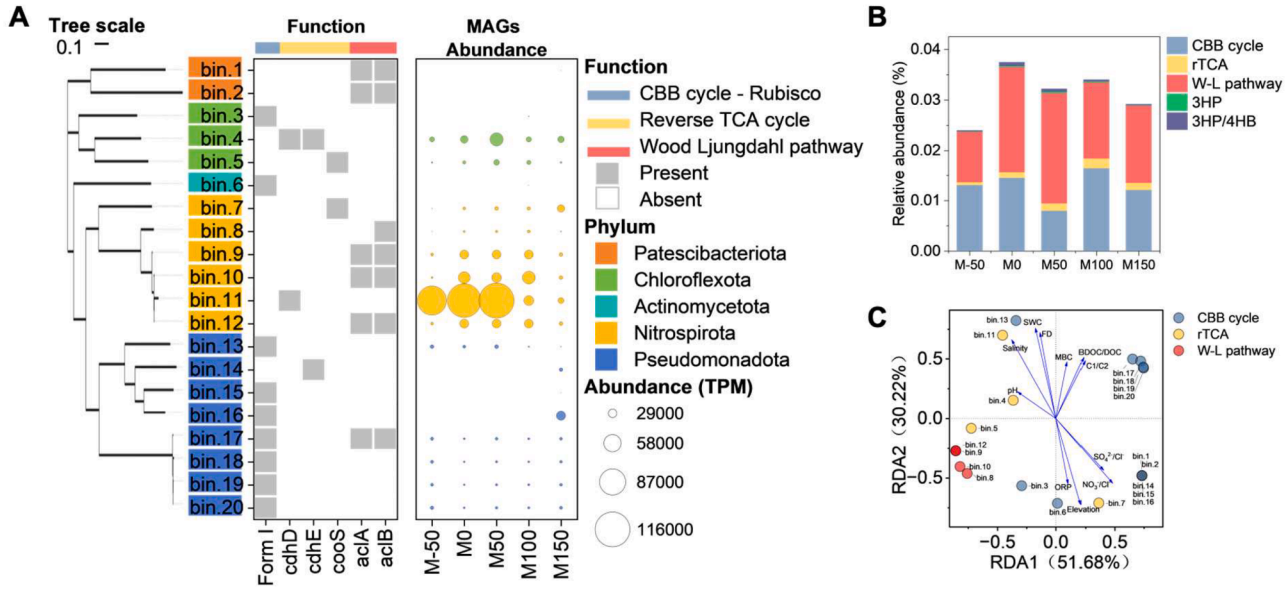


Fig. 5. Functional microorganisms related to carbon fixation in unvegetated tidal-flat sediments without vegetation cover. (A) Carbon-fixation-related MAGs. From left to right: phylogenetic tree, presence/absence of key functional genes for three carbon fixation pathways in the MAGs, and TPM abundance of MAGs along the elevation gradient. (B) Relative abundance of key functional genes for each carbon fixation pathway based on clean reads along the elevation gradient. (C) Redundancy analysis (RDA) showing the relationships between the abundance of MAGs carrying carbon fixation pathways and sediment porewater geochemical variables. Arrows indicate environmental gradients, and their lengths represent the strength of correlations with microbial community composition. The directions of arrows reflect the relationships between environmental variables and microbial taxa. Only environmental variables that were significant in permutation tests ($P < 0.05$) are shown.

3.4. Key drivers of sediment CO_2 fluxes

To identify the primary drivers of CO_2 fluxes, separate models were constructed for the dry season and wet season datasets (Fig. 6 A, B). During the dry season, SWC, elevation, and salinity were the most influential variables determining model prediction accuracy, jointly explaining > 40%. In addition, the SO_4^{2-}/Cl^- ratio and MBC also contributed to model performance to a lesser extent (Fig. 6 A). In the wet

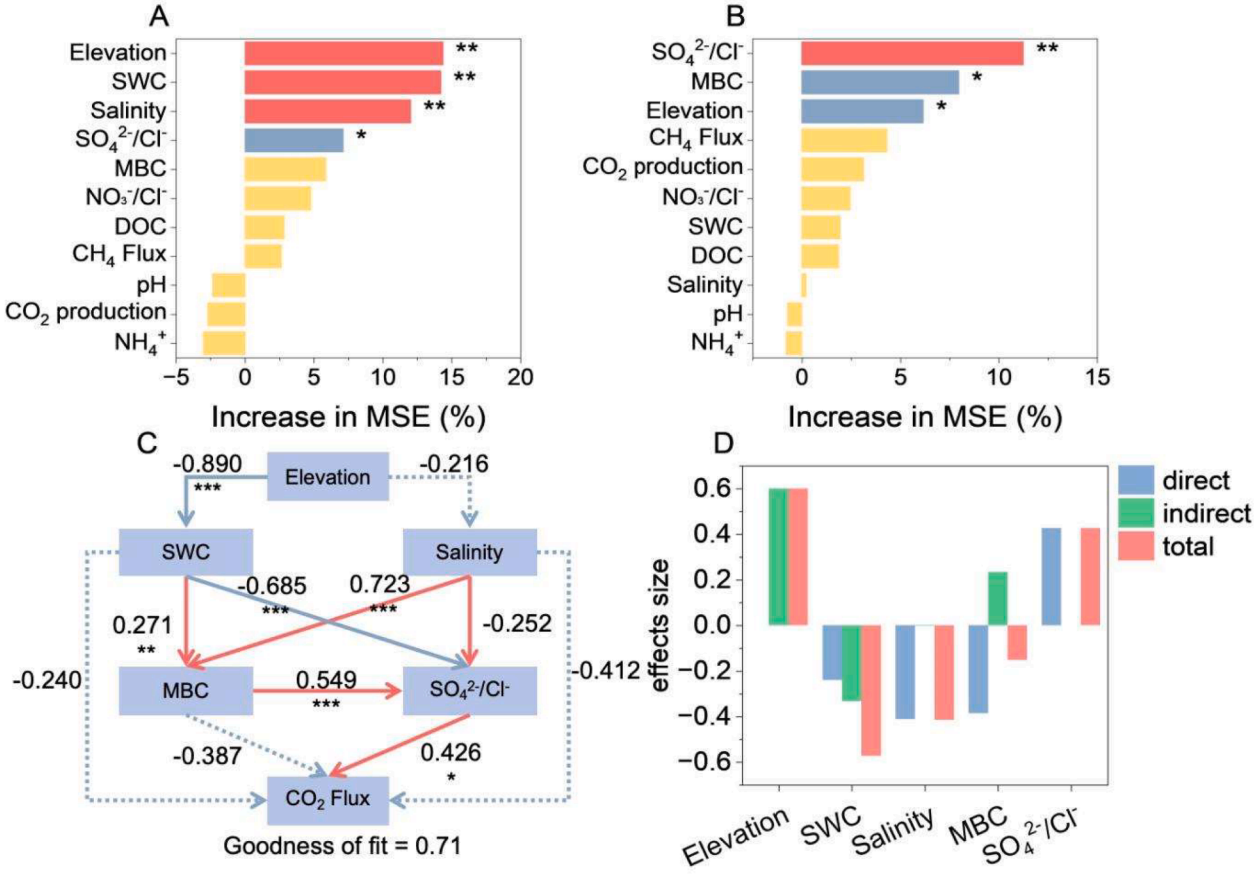


Fig. 6. Regulation of CO_2 fluxes by biogeochemical processes. (A) and (B) Random forest analysis showing the explained variance in CO_2 fluxes during the dry and wet seasons. (C) PLS-SEM illustrating the regulatory pathways through which biogeochemical properties influence CO_2 fluxes. (D) Summary of the effects of biogeochemical properties on CO_2 fluxes.

season, elevation, MBC, and SO_4^{2-}/Cl^- became the most important predictors, again explaining more than 40% of the variance ($P < 0.05$ or $P < 0.01$). Notably, the importance of MBC increased markedly compared with the dry season (Increase in MSE = 7.97, $P < 0.05$).

Based on the key predictors identified by the random forest analysis, a partial least squares structural equation model (PLS-SEM) was constructed to evaluate the relationships among environmental variables, microbial parameters, and CO_2 fluxes (GOF = 0.71; Fig. 6 C, D). The results indicated that, except for SO_4^{2-}/Cl^-, the direct effects of SWC, salinity, and MBC on CO_2 fluxes were not statistically significant. However, indirect effects mediated through intermediate variables were substantial. Elevation exerted a strong positive total effect on CO_2 fluxes (total effect = 0.60). Although SWC showed a negative direct effect on CO_2 fluxes, its indirect pathways via MBC and SO_4^{2-}/Cl^- resulted in an overall negative total effect (total effect = -0.57).

4. Discussion

4.1. Inundation threshold of CO_2 uptake in tidal-flat sediments

Sediment–atmosphere CO_2 fluxes decreased with increasing inundation frequency along the elevation gradient. Our *in-situ* observations from the marsh organ experiment in the Zhangjiang Estuary showed that CO_2 fluxes declined progressively as elevation decreased (Fig. 2 A). This pattern is consistent with previous field observations and controlled experiments conducted in tidal flat ecosystems. For example, along natural elevation gradients in the Yellow River Delta wetland, CO_2 emission fluxes decrease significantly with declining surface elevation (Wei et al., 2020). Similarly, microcosm experiments manipulating inundation depth have shown that ecosystem CO_2 fluxes under 10-40 cm water depth are significantly lower than those observed under 0-5 cm conditions (Zhao et al., 2023). Studies using marsh organs have further identified critical water-level thresholds at which vegetated ecosystems shift from CO_2 sources to sinks under 0-20 cm inundation depths (L. Wang et al., 2025). Likewise, *in situ* water-level manipulation experiments in the Yangtze River estuary wetlands demonstrated that soil respiration rates under high-water treatments are significantly lower than those under low-water conditions (Li et al., 2022). Collectively, these studies consistently indicate that water level dynamics, through their control of inundation depth and frequency, represent a primary physical driver regulating the direction and magnitude of CO_2 exchange between tidal-flat sediments and the atmosphere.

Our experimental observations further suggest that frequent inundation can support the development of CO_2 sink behavior in unvegetated tidal-flat sediments. This pattern was further supported by long-term field observations. Seasonal flux measurements conducted in the Zhangjiang Estuary tidal flats during 2024 repeatedly recorded negative CO_2 fluxes (Fig. S3), suggesting that this process is not an isolated outcome of short-term experimental conditions. Furthermore, a synthesis of published CO_2 flux observations across multiple unvegetated tidal-flat systems worldwide reveals that negative fluxes frequently occur (Wang et al., 2026). Together, these results indicate that hydrological conditions can strongly contribute to directional shifts in CO_2 fluxes in unvegetated tidal-flat sediments.

In the Zhangjiang Estuary marsh organ experiment, sediment-atmosphere CO_2 fluxes shifted from positive to negative values between 50 and 100 cm elevation, corresponding to an inundation frequency of approximately 12-28% (Fig. 2A). To further quantify this

transition, we fitted generalized additive models (GAM) to the observed relationship between CO_2 flux and annual inundation frequency and identified the source-sink transition point as the inundation frequency at which the fitted CO_2 flux crossed zero. The model-derived transition ranges were 10-16% in the dry season and 10-22% in the wet season (Fig. S4 A). The apparent difference between the treatment-based range of 12-28% and the GAM-derived range reflects the distinction between the discrete elevation interval over which the sign change was observed and the model-estimated zero-crossing range. The threshold was therefore characterized as a site-specific transition range of approximately 10-30%, rather than a universal fixed value. When CH_4 emissions were incorporated into the GWP calculation, the transition range remained broadly similar (Fig. S4 B), suggesting that CH_4 did not substantially alter the hydrological threshold in this experiment. However, this threshold is specific to the local tidal frame, sediment elevation setting, and geomorphology of the Zhangjiang Estuary marsh organ experiment. The exact threshold may vary among systems depending on tidal range, sediment type, salinity regime, drainage conditions, organic matter availability, and local redox dynamics. Therefore, the broader implication of our results is not that a universal inundation threshold applies globally, but rather that hydrological transition ranges may regulate CO_2 source-sink shifts in unvegetated tidal-flat sediments.

In terms of flux magnitude, the CO_2 uptake rates of unvegetated tidal-flat sediments are substantially lower than vegetated coastal wetlands, amounting to only ~7-22% of the median uptake fluxes reported for global mangrove and salt marsh ecosystems (Duarte et al., 2013). This magnitude is broadly consistent with previous large-scale observational studies, which estimated that net primary production by unvegetated tidal flats represents approximately 10-20% of that observed in vegetated coastal wetlands (Lin et al., 2020). However, given the extensive global area of tidal flats and the observation that CO_2 uptake can occur even under relatively modest inundation frequencies, the cumulative effect of these systems may still exert a non-negligible and potentially nonlinear influence on regional and global coastal carbon budgets.

It should also be noted that net atmospheric CO_2 uptake does not necessarily translate directly into long-term carbon sequestration. Long-term carbon storage depends on the subsequent fate of the absorbed carbon, including microbial assimilation, stabilization within sediment organic matter pools, carbonate-system dynamics, lateral export, and eventual burial. Although our results demonstrate that frequently inundated tidal-flat sediments can function as net atmospheric CO_2 sinks, the persistence of this sink and its contribution to long-term carbon sequestration remain uncertain. Future studies combining carbon burial measurements, sediment carbon accumulation rates, isotopic tracers, and longer-term observations are needed to determine how much of the absorbed CO_2 is ultimately retained over climatically relevant timescales.

4.2. *Coupling between the porewater CO_2 dissolution and microbial carbon fixation*

Changes in porewater carbonate chemistry appear to be an important contributor to the observed CO_2 uptake. Along the elevation gradient, increasing inundation was accompanied by rising porewater pH, dissolved CO_2, estimated alkalinity,(Fig. 3 D-F). Meanwhile, the potential CO_2 production rate decreased (Fig. 2B), suggesting a shift toward enhanced CO_2 accumulation and retention within porewater under more frequently inundated conditions. These patterns are consistent with theoretical expectations of the alkalinity pump (Sulpis and Middelburg, 2023). Increased alkalinity can enhance the capacity of porewater to dissolve and retain CO_2, thereby favoring atmospheric CO_2 uptake into the sediment-porewater system.

The increase in estimated alkalinity toward lower elevations likely reflects the combined effects of multiple interacting geochemical processes. Carbonate dissolution can increase both alkalinity and DIC where carbonate minerals are available, although the relatively stable Ca^{2+} and Mg^{2+} concentrations along the elevation gradient in our experiment suggest that this process was unlikely to be the sole dominant driver (Fig. 3C). Salinity-driven ion exchange may also modify porewater pH and carbonate speciation. However, porewater salinity showed no significant differences among elevation treatments in our experience. Organic matter mineralization can supply porewater CO_2, and when coupled with anaerobic redox processes—including denitrification, sulfate reduction, and potentially iron and manganese reduction—it may also alter alkalinity production and proton consumption.

In this study, the marked decline in SO_4^{2-}/Cl^- ratios, together with the enrichment of sulfate-reduction functional genes and sulfate-reducing microbial populations under higher inundation conditions (Fig. 5), is consistent with a potential contribution of sulfate reduction to alkalinity production. In addition, the elevated proportion of BDOC observed in porewater (Fig. 4 C) provides a substantial supply of electron donors. In coastal wetland sediments, sulfate reduction often dominates anaerobic mineralization of organic carbon, accounting for a large proportion of total respiration (Luo et al., 2019; Yin et al., 2021). Nevertheless, denitrification likely also plays an important role. Although porewater NO_3^- concentrations were low during sampling, the surrounding estuarine waters receive substantial external nitrate inputs (114.5-202.6 μmol L^{-1}), and previous studies have reported active denitrification processes in sediments of the Zhangjiang Estuary (Wang et al., 2023). The ratio of DIC to TA in the estuarine water column further suggests that denitrification is a dominant source of alkalinity in this area (Lu et al., 2023). Together, these results support the possibility that denitrification and sulfate reduction jointly contribute to alkalinity-associated CO_2 dissolution and retention along the elevation gradient, although direct measurements of process rates are still needed to confirm their relative contributions.

We further evaluated whether microphytobenthic photosynthesis could account for the observed negative CO_2 fluxes. Even under favorable light conditions during tidal exposure, reported maximum carbon fixation rates of benthic microalgae are typically up to ~180 mg C m^{-2} h^{-1}, with most values remaining below 50 mg C m^{-2} h^{-1} (MacIntyre et al., 1996; Middelburg et al., 2000). These rates are substantially lower than the CO_2 uptake flux observed in this study, which reached up to -303 mg C m^{-2} h^{-1} (Fig. 2 A). More importantly, photosynthesis produces oxygen, whereas our observations show a decline in sediment Eh and substantial sulfate consumption along the elevation gradient (Fig. 1; Fig. 3), indicating oxygen-limited conditions. If microphytobenthic photosynthesis were the dominant driver, stronger CO_2 uptake would be expected at higher elevations with longer exposure and greater light availability; however, the strongest net CO_2 uptake occurred at lower elevations with more frequent inundation and more reducing conditions. These results suggest that microphytobenthic photosynthesis alone is unlikely to explain the magnitude and elevation dependence of the observed CO_2 uptake.

Anaerobic conditions also reshape carbon fixation microbial communities with great potential for energy-efficient strategies (Liu et al., 2022). Metagenomic analyses revealed that microbial communities in frequently inundated, low-elevation sediments were enriched in MAGs carrying genes associated with the rTCA cycle (Fig. 5). This observation is consistent with previous studies showing that dark carbon fixation in coastal sediments increases with decreasing oxygen availability and water depth (Vasquez-Cardenas et al., 2020), but in our study it should be interpreted as evidence of metabolic potential rather than direct evidence of realized in situ activity.

Despite this shift, the direct contribution of microbial autotrophic fixation to the observed negative CO_2 fluxes is likely limited. First, the relative abundance of genes encoding autotrophic carbon fixation pathways was substantially lower than that of genes associated with heterotrophic organic matter mineralization. Second, from an energetic perspective, heterotrophic respiration processes such as sulfate reduction and denitrification typically yield higher energy returns than

chemolithoautotrophic carbon fixation, particularly in sediments rich in labile organic substrates (Thauer et al., 1977). Moreover, previously reported rates of dark carbon fixation in sediments are generally much lower than the net CO_2 uptake flux observed in this study (Liu et al., 2024). Therefore, while microbial autotrophic pathways may not directly drive the bulk CO_2 uptake, they likely represent an important functional component of the anaerobic metabolic network, potentially contributing to microbial biomass production and carbon retention under frequent inundation. Direct quantification of realized microbial carbon-fixation activity would require transcriptomic, enzymatic, or stable-isotope evidence.

Finally, anaerobic conditions may enhance microbial carbon retention by altering the balance between organic matter mineralization and biomass production. Along the elevation gradient, potential CO_2 production rates declined significantly with increasing inundation (Fig. 2 B), while MBC increased (Fig. 4 A), suggesting that a greater fraction of carbon is assimilated into biomass rather than released as CO_2. CAZyme annotations further show enrichment of enzymes involved in anaerobic degradation of complex plant-derived polysaccharides in low-elevation sediments (Fig. S5), indicating efficient utilization of recalcitrant substrates. Consistently, dissolved organic matter fluorescence shifted from protein-like to humic-like components during incubation (Fig. 4 D), suggesting the formation of more stable organic matter. Previous studies similarly report higher carbon use efficiency (CUE) in microbial communities shaped by frequent inundation (Tan et al., 2025). Together, these patterns indicate that tidally driven anaerobic conditions enhance carbon retention through higher CUE, biomass production, and organic matter stabilization.

4.3. Limitations and future perspectives

Although this study provides multiple lines of evidence revealing the mechanisms through which unvegetated tidal flats can function as an atmospheric CO_2 sink, several limitations should be acknowledged, which also highlight important directions for future research.

First, the marsh-organ design isolates the incubation containers from the underlying natural sediments, thereby removing important lateral hydrological and biogeochemical transport processes that occur in natural tidal flats. Consequently, the system may underestimate net greenhouse gas exchange, particularly CH_4 emissions.

Second, the small sample size is a common limitation in marsh organ experiments. This limitation, together with the short tidal sampling window and limited extractable porewater volume, prevented us from obtaining sufficient porewater for direct total alkalinity titration. In addition, metagenomic analysis characterizes the functional gene potential of microbial communities rather than their real-time transcriptional activity or enzyme expression (Louca et al., 2016; Uchiyama and Miyazaki, 2009). Future studies could address these uncertainties through direct total alkalinity measurements, porewater DIC characterization, rate measurements of denitrification and sulfate reduction, metatranscriptomic or metaproteomic analyses, and stable-isotope labeling experiments to directly quantify in situ dark carbon fixation and other carbon transformation pathways.

Third, gas flux measurements were conducted mainly during tidal exposure, and high-frequency observations across the full inundation–exposure cycle were lacking. Although geochemical evidence suggests activation of the alkalinity pump during inundation, the duration and magnitude of net carbon uptake remain uncertain. Previous mesocosm studies indicate that inundation can suppress CO_2 emissions (Li et al., 2022). Continuous in situ monitoring across complete tidal cycles is therefore needed to verify this hypothesis.

5. Conclusion

This study integrates CO_2 and CH_4 flux measurements, porewater geochemistry, carbonate-system calculations, and metagenomic sequencing to examine how hydrological regimes regulate carbon exchange in unvegetated tidal flats sediments. Our results identify a site-specific hydrological source–sink transition in which sediments shifted from weak net CO_2 release to net CO_2 uptake around an annual inundation frequency of approximately 30% within the local tidal frame of the Zhangjiang Estuary. This transition was accompanied by a coupled geochemical-microbial mechanism. Frequent inundation enhances anaerobic respiration (denitrification and sulfate reduction), generating alkalinity that promotes CO_2 dissolution into porewater. The accumulation of porewater CO_2 coincided with enriched rTCA cycle related carbon-fixation potential and increased microbial biomass carbon, suggesting a possible link between porewater CO_2 retention and microbial carbon assimilation under frequent inundation. Together, these findings reveal that hydrological modulation of geochemical and microbial processes enables unvegetated tidal-flat sediments to function as CO_2 sinks. These insights call for integrating hydrological and microbial mechanisms into blue carbon assessments, particularly in unvegetated tidal flat systems that have been largely overlooked.

CRediT authorship contribution statement

Hui Wu: Conceptualization, Data curation, Formal analysis, Investigation, Methodology, Validation, Visualization, Writing – original draft, Writing – review & editing. **Yasong Chen:** Conceptualization, Investigation, Methodology, Validation, Writing – original draft. **Shiyao Chen:** Investigation, Validation, Writing – review & editing. **Mengru Li:** Investigation, Writing – review & editing. **Yihui Zhang:** Conceptualization, Methodology, Validation, Visualization, Writing – review & editing. **Mingliang Zhao:** Methodology, Validation, Visualization, Writing – review & editing. **Guangxuan Han:** Conceptualization, Methodology, Writing – review & editing. **Nengwang Chen:** Conceptualization, Methodology, Validation, Visualization, Writing – review & editing.

Declaration of competing interest

The authors declare that they have no known competing financial interests or personal relationships that could have appeared to influence the work reported in this paper.

Acknowledgments

This work was supported by the National Key R&D Program of China (2022YFF0802102); the National Natural Science Foundation of China (42530405); the Shenzhen Science and Technology Plan Project (KCXST20221021111404011), and MEL Internal Program (No. MELRI2501). We are grateful to Wenhong Xu, Wenyan Tang, Hao Pan, Shengyuan Tang, Yuanhao Cao, Chunyan Cheng, Ting Jiang, Yu Cai, Zheng Wang and Yuyang Zheng for their help in field measurement, and to Liyang Zhan, Qiang Zheng, Yuanmin Sun, Yong Ma, Junhui Chen, Fang Wu, Junou Du, and Lei Wang for their supportive technician work.

Supplementary materials

Supplementary material associated with this article can be found, in the online version, at doi:10.1016/j.watres.2026.126544.

Data availability

Data will be made available on request.

References

Alongi, D.M., 2014. Carbon cycling and storage in mangrove forests. Annu. Rev. Mar. Sci. 6, 195–219. https://doi.org/10.1146/annurev-marine-010213-135020.

Berg, I.A., 2011. Ecological aspects of the distribution of different autotrophic CO_2 fixation pathways. Appl. Environ. Microbiol. 77, 1925–1936. https://doi.org/10.1128/aem.02473-10.

Bertram, C., Quaas, M., Reusch, T.B.H., Vafeidis, A.T., Wolff, C., Rickels, W., 2021. The blue carbon wealth of nations. Nat. Clim. Change 11, 704–709. https://doi.org/10.1038/s41558-021-01089-4.

Candry, P., Abrahamson, B., Stahl, D.A., Winkler, M.-K.H., 2023. Microbially mediated climate feedbacks from wetland ecosystems. Global Change Biol. 29, 5169–5183. https://doi.org/10.1111/gcb.16850.

Chen, Z.L., Lee, S.Y., 2024. Carbon dioxide fluxes from peri-urban tidal flats in South China. Estuaries Coasts. 47, 2238–2252. https://doi.org/10.1007/s12237-024-01405-z.

Cotovicz, L.C., Abril, G., Sanders, C.J., Tait, D.R., Maher, D.T., Sippo, J.Z., Holloway, C., Yau, Y.Y.Y., Santos, I.R., 2024. Methane oxidation minimizes emissions and offsets to carbon burial in mangroves. Nat. Clim. Change 14, 275–281. https://doi.org/10.1038/s41558-024-01927-1.

Davidson, N.C., Finlayson, C.M., 2019. Updating global coastal wetland areas presented in Davidson and Finlayson (2018). Mar. Freshwater Res. 70, 1195–1200. https://doi.org/10.1071/MF19010.

Dong, J., Chen, X., Chen, F., Hu, Z., Tu, Q., Li, G., He, C., Shi, Q., Zheng, Q., Chen, F., Shi, T., Jiao, N., Liu, J., 2026. Temperature thresholds govern microbial-mediated dissolved organic carbon dynamics in coastal ecosystems. Adv. Sci. 13, e11348. https://doi.org/10.1002/advs.202511348.

Douglas, E.J., Lam-Gordillo, O., Hailes, S.F., Lohrer, A.M., Cummings, V.J., 2025. Simulated heatwave alters intertidal estuary greenhouse gas fluxes. Nat. Commun. 16, 10507. https://doi.org/10.1038/s41467-025-65519-z.

Duarte, C.M., Losada, I.J., Hendriks, I.E., Mazarrasa, I., Marbà, N., 2013. The role of coastal plant communities for climate change mitigation and adaptation. Nat. Clim. Change 3, 961–968. https://doi.org/10.1038/NCLIMATE1970.

Falkowski, P.G., Fenchel, T., Delong, E.F., 2008. The microbial engines that drive Earth's biogeochemical cycles. Science 320, 1034–1039. https://doi.org/10.1126/science.1153213.

Fan, Y., Zhou, Z., Liu, F., Qian, L., Yu, X., Huang, F., Hu, R., Su, H., Gu, H., Yan, Q., He, Z., Wang, C., 2024. The vertical partitioning between denitrification and dissimilatory nitrate reduction to ammonium of coastal mangrove sediment microbiomes. Water Res. 262, 122113. https://doi.org/10.1016/j.watres.2024.122113.

Fuchs, G., 2011. Alternative pathways of carbon dioxide fixation: insights into the early evolution of life? Annu. Rev. Microbiol. 65, 631–658. https://doi.org/10.1146/annurev-micro-090110-102801.

Guo, W., Yang, L., Hong, H., Stedmon, C.A., Wang, F., Xu, J., Xie, Y., 2011. Assessing the dynamics of chromophoric dissolved organic matter in a subtropical estuary using parallel factor analysis. Mar. Chem. 124, 125–133. https://doi.org/10.1016/j.marchem.2011.01.003.

Hamilton, D.J., Bulmer, R.H., Schwendenmann, L., Lundquist, C.J., 2020. Nitrogen enrichment increases greenhouse gas emissions from emerged intertidal sandflats. Sci. Rep. 10, 6686. https://doi.org/10.1038/s41598-020-62215-4.

Hu, X., Cai, W.J., 2011. An assessment of ocean margin anaerobic processes on oceanic alkalinity budget. Glob. Biogeochem. Cycl. 25, n/a-n/a. https://doi.org/10.1029/2010GB003859.

Jørgensen, L., Stedmon, C.A., Kragh, T., Markager, S., Middelboe, M., Søndergaard, M., 2011. Global trends in the fluorescence characteristics and distribution of marine dissolved organic matter. Mar. Chem. 126, 139–148. https://doi.org/10.1016/j.marchem.2011.05.002.

Krauss, K.W., Holm, G.O., Perez, B.C., McWhorter, D.E., Cormier, N., Moss, R.F., Johnson, D.J., Neubauer, S.C., Raynie, R.C., 2016. Component greenhouse gas fluxes and radiative balance from two deltaic marshes in Louisiana: pairing chamber techniques and eddy covariance. J. Geophys. Res. Biogeosci. 121, 1503–1521. https://doi.org/10.1002/2015JG003224.

Lewis, E., Wallace, D.W.R., 1998. Program developed for CO_2 system calculations. Carbon Dioxide Information Analysis Center. Oak Ridge National Laboratory, Oak Ridge, TN. https://doi.org/10.15485/1464255.

Li, Y.L., Ge, Z.M., Xie, L.N., Li, S.H., Tan, L-S., 2022. Effects of waterlogging and salinity increase on CO_2 efflux in soil from coastal marshes. Appl. Soil Ecol. 170, 104268. https://doi.org/10.1016/j.apsoil.2021.104268.

Lian, J., Zheng, X., Zhuo, X., Chen, Y.L., He, C., Zheng, Q., Lin, T.-H., Sun, J., Guo, W., Shi, Q., Jiao, N., Cai, R., 2021. Microbial transformation of distinct exogenous substrates into analogous composition of recalcitrant dissolved organic matter. Environ. Microbiol. 23, 2389–2403. https://doi.org/10.1111/1462-2920.15426.

Lin, W.J., Wu, J., Lin, H.J., 2020. Contribution of unvegetated tidal flats to coastal carbon flux. Glob. Change Biol. 26, 3443–3454. https://doi.org/10.1111/gcb.15107.

Liu, B., Hou, L., Zheng, Y., Zhang, Z., Tang, X., Mao, T., Du, J., Bi, Q., Dong, H., Yin, G., Han, P., Liang, X., Liu, M., 2022. Dark carbon fixation in intertidal sediments: Controlling factors and driving microorganisms. Water Res. 216, 118381. https://doi.org/10.1016/j.watres.2022.118381.

Liu, B., Qi, L., Zheng, Y., Zhang, C., Zhou, J., An, Z., Wang, B., Lin, Z., Yao, C., Wang, Y., Yin, G., Dong, H., Li, X., Liang, X., Han, P., Liu, M., Zhang, G., Cui, Y., Hou, L., 2024. Four years of climate warming reduced dark carbon fixation in coastal wetlands. ISME J. 18. https://doi.org/10.1093/ismejo/wrae138.

Liu, S., Jiang, Z., Zhang, J., Wu, Y., Huang, X., Macreadie, P.I., 2017. Sediment microbes mediate the impact of nutrient loading on blue carbon sequestration by mixed seagrass meadows. Sci. Total Environ. 599-600, 1479–1484. https://doi.org/10.1016/j.scitotenv.2017.05.129.

Louca, S., Parfrey, L.W., Doebeli, M., 2016. Decoupling function and taxonomy in the global ocean microbiome. Science 353, 1272–1277. https://doi.org/10.1126/science.aaf4507.

Lovelock, C.E., Cahoon, D.R., Friess, D.A., Guntenspergen, G.R., Krauss, K.W., Reef, R., Rogers, K., Saunders, M.L., Sidik, F., Swales, A., Saintilan, N., Thuyen, L.X., Triet, T., 2015. The vulnerability of indo-pacific mangrove forests to sea-level rise. Nature 526, 559–563. https://doi.org/10.1038/nature15538.

Lu, Z., Wang, F., Xiao, K., Wang, Y., Yu, Q., Cheng, P., Chen, N., 2023. Carbon dynamics and greenhouse gas outgassing in an estuarine mangrove wetland with high input of riverine nitrogen. Biogeochemistry 162, 221–235. https://doi.org/10.1007/s10533-022-00999-5.

Luo, M., Zhu, W., Huang, J., Liu, Y., Duan, X., Wu, J., Tong, C., 2019. Anaerobic organic carbon mineralization in tidal wetlands along a low-level salinity gradient of a subtropical estuary: Rates, pathways, and controls. Geoderma 337, 1245–1257. https://doi.org/10.1016/j.geoderma.2018.07.030.

MacIntyre, H.L., Geider, R.J., Miller, D.C., 1996. Microphytobenthos: the ecological role of the "secret garden" of unvegetated, shallow-water marine habitats. i. distribution, abundance and primary production. Estuaries 19, 186. https://doi.org/10.2307/1352224.

Macreadie, P.I., Anton, A., Raven, J.A., Beaumont, N., Connolly, R.M., Friess, D.A., Kelleway, J.J., Kennedy, H., Kuwae, T., Lavery, P.S., Lovelock, C.E., Smale, D.A., Apostolaki, E.T., Atwood, T.B., Baldock, J., Bianchi, T.S., Chmura, G.L., Eyre, B.D., Fourqurean, J.W., Hall-Spencer, J.M., Huxham, M., Hendriks, I.E., Krause-Jensen, D., Laffoley, D., Luisetti, T., Marbà, N., Masque, P., McGlathery, K.J., Megonigal, J.P., Murdiyarso, D., Russell, B.D., Santos, R., Serrano, O., Silliman, B.R., Watanabe, K., Duarte, C.M., 2019. The future of blue carbon science. Nat. Commun. 10, 3998. https://doi.org/10.1038/s41467-019-11693-w.

Megonigal, J.P., Hines, M.E., Visscher, P.T., 2003. Anaerobic metabolism: linkages to trace gases and aerobic processes. In: Schlesinger, W.H. (Ed.), Biogeochemistry. Elsevier-Pergamon, Oxford, pp. 317–424. https://doi.org/10.1016/B0-08-043751-6/08132-9.

Middelburg, J.J., 2011. Chemoautotrophy in the ocean. Geophys. Res. Lett. 38, n/a-n/a. https://doi.org/10.1029/2011GL049725.

Middelburg, J.J., Barranguet, C., Boschker, H.T.S., Herman, P.M.J., Moens, T., Heip, C.H.R., 2000. The fate of intertidal microphytobenthos carbon: an in situ ^{13}C-labeling study. Limnol. Oceanogr. 45, 1224–1234. https://doi.org/10.4319/lo.2000.45.6.1224.

Middelburg, J.J., Soetaert, K., Hagens, M., 2020. Ocean alkalinity, buffering and biogeochemical processes. Rev. Geophys. 58. https://doi.org/10.1029/2019RG000681 e2019RG000681.

Murray, N.J., Phinn, S.R., DeWitt, M., Ferrari, R., Johnston, R., Lyons, M.B., Clinton, N., Thau, D., Fuller, R.A., 2019. The global distribution and trajectory of tidal flats. Nature 565, 222–225. https://doi.org/10.1038/s41586-018-0805-8.

Qi, L., Zheng, Y., Hou, L., Liu, B., Zhou, J., An, Z., Wu, L., Chen, F., Lin, Z., Yin, G., Dong, H., Li, X., Liang, X., Liu, M., 2023. Potential response of dark carbon fixation to global warming in estuarine and coastal waters. Glob. Change Biol. 29, 3821–3832. https://doi.org/10.1111/gcb.16702.

Shahan, J., Chu, H., Windham-Myers, L., Matsumura, M., Carlin, J., Eichelmann, E., Stuart-Haentjens, E., Bergamaschi, B., Nakatsuka, K., Sturtevant, C., Oikawa, P., 2022. Combining eddy covariance and chamber methods to better constrain CO_2 and CH_4 fluxes across a heterogeneous restored tidal wetland. J. Geophys. Res.: Biogeosci. 127. https://doi.org/10.1029/2022JG007112 e2022JG007112.

Steffens, L., Pettinato, E., Steiner, T.M., Mall, A., König, S., Eisenreich, W., Berg, I.A., 2021. High CO_2 levels drive the TCA cycle backwards towards autotrophy. Nature 592, 784–788. https://doi.org/10.1038/s41586-021-03456-9.

Su, G., Guo, Z., Hu, Y., Zheng, Q., Zopfi, J., Lehmann, M.F., Jiao, N., 2024. Tidal control on aerobic methane oxidation and mitigation of methane emissions from coastal mangrove sediments. Environ. Res. 263, 120049. https://doi.org/10.1016/j.envres.2024.120049.

Sulpis, O., Middelburg, J.J., 2023. Inorganic blue carbon sequestration. Nat. Sustain. 6, 1039–1040. https://doi.org/10.1038/s41893-023-01143-3.

Tan, J., Huang, J., Quan, W., Su, L., Liu, Y., Cai, Y., Li, S., Guo, P., Luo, M., 2025. Divergence of microbial carbon use efficiency and soil organic carbon along a tidal flooding gradient in a subtropical coastal wetland. Water Res. 280, 123527. https://doi.org/10.1016/j.watres.2025.123527.

Thauer, R.K., Jungermann, K., Decker, K., 1977. Energy conservation in chemotrophic anaerobic bacteria. Bacteriol. Rev. 41, 100–180. https://doi.org/10.1128/br.41.1.100-180.1977.

Uchiyama, T., Miyazaki, K., 2009. Functional metagenomics for enzyme discovery: challenges to efficient screening. Curr. Opin. Biotechnol. 20, 616–622. https://doi.org/10.1016/j.copbio.2009.09.010.

Vasquez-Cardenas, D., Meysman, F.J.R., Boschker, H.T.S., 2020. A cross-system comparison of dark carbon fixation in coastal sediments. Glob. Biogeochem. Cycl. 34. https://doi.org/10.1029/2019GB006298 e2019GB006298.

Wang, F., Lu, Z., Tobias, C.R., Wang, Y., Xiao, K., Yu, Q., Lin, J., Huang, G., Chen, N., 2023. Salt marsh expansion into estuarine mangrove mudflats reduces nitrogen removal capacity. CATENA 232, 107459. https://doi.org/10.1016/j.catena.2023.107459.

Wang, J., Chen, X., Wang, Y., Chen, Y., Wu, H., Wittyngham, S.S., Kirwan, M.L., Zhang, Y., Liu, W., Zhang, Y., 2025. Life-history plasticity of intertidal salt marsh in response to sea level rise: Salinity and inundation modulate size-dependent flowering of Spartina alterniflora. Ecol. Indic. 177, 113790. https://doi.org/10.1016/j.ecolind.2025.113790.

Wang, L., Zhao, M., Nie, M., Paytan, A., Santos, I.R., Wang, X., Cao, Q., Song, W., Chu, X., Han, G., 2025. Thresholds of wetland carbon sink regulation by water level. Environ. Sci. Technol. 59, 13811–13819. https://doi.org/10.1021/acs.est.5c03410.

Wang, Y., Li, C., Peng, Z., Luo, J., Zhu, S., Sun, Y., Liu, R., Jiang, D., Zhou, X., Wang, F., 2026. Unvegetated tidal flats: a critical yet vulnerable coastal blue carbon sink. Glob. Change Biol. 32, e70695. https://doi.org/10.1111/gcb.70695.

Wei, S., Han, G., Chu, X., Song, W., He, W., Xia, J., Wu, H., 2020. Effect of tidal flooding on ecosystem CO_2 and CH_4 fluxes in a salt marsh in the yellow river delta. Estuar. Coast. Shelf Sci. 232, 106512. https://doi.org/10.1016/j.ecss.2019.106512.

Weiss, R.F., 1974. Carbon dioxide in water and seawater: The solubility of a non-ideal gas. Mar. Chem. 2, 203–215. https://doi.org/10.1016/0304-4203(74)90015-2.

Yin, X., Lin, Y., Li, Y., Wang, L., Sun, Z., Li, G., 2021. Sulfate reduction and its important role in organic carbon mineralization in sediments of the pearl river Estuary. Estuarine Coast. Shelf Sci. 260, 107511. https://doi.org/10.1016/j.ecss.2021.107511.

Zhao, M., Li, P., Song, W., Chu, X., Eller, F., Wang, X., Liu, J., Xiao, L., Wei, S., Li, X., Han, G., 2023. Inundation depth stimulates plant-mediated CH_4 emissions by increasing ecosystem carbon uptake and plant height in an estuarine wetland. Funct. Ecol. 37, 536–550. https://doi.org/10.1111/1365-2435.14258.

Zhu, X., Qin, Z., Liu, W., Kirwan, M.L., Lu, H., Lee, S.Y., Dai, M., 2025. Coastal restoration may not necessarily enhance blue carbon sink. Geophys. Res. Lett. 52. https://doi.org/10.1029/2025GL114614 e2025GL114614.